










ORIGINAL
ARTICLE

Delivery of an anti-transthyretin Nanobody to the brain through intranasal administration reveals transthyretin expression and secretion by motor neurons

João R. Gomes*[†] , Inês Cabrito[‡] , Hugo R. Soares[‡] ,
Susete Costelha*[†] , Anabela Teixeira*[†] , Angela Wittelsberger[‡] ,
Catelijne Stortelers[‡] , Peter Vanlandschoot[‡]¹  and Maria J. Saraiva*[†] 

**Instituto de Investigação e Inovação em Saúde (I3S), University of Porto, Porto, Portugal*

[†]*Neurobiology Unit, IBMC- Institute for Molecular and Cell Biology, University of Porto, Porto, Portugal*

[‡]*ABLYNX, Ghent, Belgium*

Abstract

Transthyretin (TTR) is a transport protein of retinol and thyroxine in serum and CSF, which is mainly secreted by liver and choroid plexus, and in smaller amounts in other cells throughout the body. The exact role of TTR and its specific expression in Central Nervous System (CNS) remains understudied. We investigated TTR expression and metabolism in CNS, through the intranasal and intracerebroventricular delivery of a specific anti-TTR Nanobody to the brain, unveiling Nanobody pharmacokinetics to the CNS. In TTR deficient mice, we observed that anti-TTR Nanobody was successfully distributed throughout all brain areas, and also reaching the spinal cord. In wild-type mice, a similar distribution pattern was observed. However, in areas known to be rich in TTR, reduced levels of Nanobody were found, suggesting potential target-mediated effects. Indeed, in wild-type mice, the anti-TTR

Nanobody was specifically internalized in a receptor-mediated process, by neuronal-like cells, which were identified as motor neurons. Whereas in KO TTR mice Nanobody was internalized by all cells, for late lysosomal degradation. Moreover, we demonstrate that *in vivo* motor neurons also actively synthesize TTR. Finally, *in vitro* cultured primary motor neurons were also found to synthesize and secrete TTR into culture media. Thus, through a novel intranasal CNS distribution study with an anti-TTR Nanobody, we disclose a new cell type capable of synthesizing TTR, which might be important for the understanding of the physiological role of TTR, as well as in pathological conditions where TTR levels are altered in CSF, such as amyotrophic lateral sclerosis.

Keywords: ALS, intranasal delivery, motor neuron, nanobody, spinal cord, transthyretin.

J. Neurochem. (2018) **145**, 393–408.

Transthyretin is a tetramer protein composed of four identical subunits, encoded by a single copy gene (Tsuzuki *et al.* 1985). It is a very well-conserved protein among species, from vertebrate to transthyretin (TTR)-like proteins in bacteria and plants (Power *et al.* 2000). It is involved in the blood transport of thyroid hormones thyroxine (T4) and retinol (vitamin A) through retinol-binding protein. TTR has been mostly studied in its mutated form, with single amino acid substitutions, which gives rise to a neurodegenerative

Received January 5, 2018; revised manuscript received February 6, 2018; accepted February 27, 2018.

Address correspondence and reprint requests to Maria João Saraiva, i3S – Instituto de Investigação e Inovação em Saúde da Universidade do Porto, Rua Alfredo Allen, 208, 4200 – 135 Porto, Portugal. E-mail: mjsaraiv@ibmc.up.pt

¹Present address: N-Spire BVBA, Aalter, Belgium

Abbreviations used: ALS, amyotrophic lateral sclerosis; CSF, cerebrospinal fluid; ICV, intracerebroventricular; TTR, transthyretin; WT, wild type.

disorder, the hereditary familial amyloid polyneuropathy (Andrade 1952), affecting small sensory neurons. This disorder is characterized by extracellular deposition of aggregates and fibrils of the mutated TTR, mainly in the nerves of the peripheral nervous system. Wild-type TTR has shown to have physiological roles in behavior, cognition, nerve regeneration, and neurite/axonal outgrowth (Alshehri *et al.* 2015) (Gomes *et al.* 2016). More importantly, TTR has shown to be a neuroprotective protein in the central nervous system (CNS), in pathologies like Alzheimer or stroke (Choi *et al.* 2007; Gomes *et al.* 2016). In ischemic conditions, TTR has shown not only to reduce the infarct volume in a mouse stroke model (Santos *et al.* 2010), but also in *in vitro* excitotoxic models; TTR rescued neurons from cell death and neurite loss by controlling cAMP-response element binding (CREB) protein and the Bcl2 protein family, demonstrating that TTR could be regarded as a neurotrophic factor (Gomes *et al.* 2016). Furthermore, TTR has shown to be a possible biomarker in amyotrophic lateral sclerosis (ALS), as TTR CSF levels were found to be altered in the proteome of CSF of ALS patients compared to healthy donors (Ranganathan *et al.* 2005; Brettschneider *et al.* 2010; Ryberg *et al.* 2010). TTR is mainly expressed and secreted by the liver and choroid plexus, sources of TTR in blood and CSF, respectively (Murakami *et al.* 1987). It is also expressed in other cells throughout the body, in smaller amounts, like in retinal pigmented cells of the eye (Kawaji *et al.* 2005), glucagon cells in pancreas (Kato *et al.* 1985), meninges (Blay *et al.* 1993), stomach, heart, muscle, and spleen (Soprano *et al.* 1985). Regarding TTR synthesis in the CNS other than in the choroid plexus, TTR has been detected in minimal amounts in brain areas such as cortex, striatum, or cerebellum (Carro *et al.* 2002; Stein and Johnson 2002; Buxbaum *et al.* 2008; Li *et al.* 2011). However, it is still not clear whether this refers to actual neuronal TTR synthesis or to contamination by the epithelial cells from choroid plexus that secrete high amounts of TTR (Sousa *et al.* 2007).

Access of the CNS for treatment of diseases is very challenging because of the presence of the blood–brain barrier (BBB). Several strategies were developed to overcome BBB and allow therapeutic substances to reach the CNS. These strategies can be more invasive, like intracerebral or intraventricular delivery (ICV), or non-invasive like intranasal administration. Intranasal administration is thus an appealing strategy owing to its non-invasive characteristics, rapid absorption, fast onset of action, and minimal systemic exposure (Furrer *et al.* 2009). However, some disadvantages are associated with intranasal delivery, namely the restricted amount of drug delivered, high inter-individual variability and low CNS delivery efficiency when compared with ICV delivery (Lochhead and Thorne 2012). Nevertheless, intranasal delivery has been well characterized for a few drugs and for small proteins, like insulin and anti-TNF (Tumor necrosis factor) scFv antibody fragment, but not for Nanobodies

(Thorne *et al.* 2004; Dhuria *et al.* 2010). These intranasal delivery studies identified two pathways: the olfactory and trigeminal nerves as means for migration from the nasal olfactory epithelium to the brain. The drugs reach mainly the olfactory bulb, brainstem, and cerebrospinal fluid, overcoming the BBB (Thorne *et al.* 2004; Dhuria *et al.* 2010).

Nanobodies® (trademark of Ablynx) correspond to the variable domain (VHH) of the heavy chain-only antibodies that are naturally occurring in *Camelidae* species, constituting small antigen-binding fragments with a molecular weight of only 12–15 kDa (Wolfson 2006). Their single domain nature and small size compared to conventional antibodies (150 kDa) are associated with many advantages, like high stability, the ability to bind ‘hard to reach’ epitopes such as enzymatic clefts and important for our study here, targeted immunolabeling and antigen manipulation in living cells (Herce *et al.* 2017) and enhanced tissue penetration. Nevertheless, despite their small size, Nanobodies have low intrinsic capacity to cross the BBB when systemically administrated (Terry *et al.* 2014) just like conventional antibodies.

In this work, we report the generation of a mouse and human cross-reactive TTR-specific Nanobody. We demonstrate that following intranasal administration, the Nanobody successfully distributed throughout distinct brain areas, reaching also the spinal cord. Using this Nanobody we further show that motor neurons in the spinal cord not only specifically internalized the Nanobody, but also synthesize TTR.

Material and methods

Mice

The number of mice handled for this research was approved by the Institutional and National General Veterinary Board Ethical Committees (approval reference number 003424), according to National and European Union rules. Three to 6-month-old TTR Wild Type (+/+), TTR KO (−/−) (Episkopou *et al.* 1993), in a 129/svJ background were used for Nanobody delivery experiments and motor neuron cultures. The animals were reproduced, maintained (regular rodents chow and tap water ad libitum) and experimentally manipulated under a 12 h light/dark cycle in type II cages in specific pathogen-free conditions in the animal facility (microbiological health status available). The method of euthanasia used was cervical displacement. Charles River Laboratories is the external animal facility used to acquire animals. Genotypes were determined from tail extracted genomic DNA, using primers for the detection of exon 2 of TTR (which is disrupted in TTR−/− by insertion of a neomycin resistance gene), as previously described (Episkopou *et al.* 1993). ARRIVE guidelines were taken into consideration in experimental reporting. This study was not pre-registered.

Anti-TTR Nanobody discovery and characterization

Two llamas were immunized with a cocktail solution of two recombinant proteins: wild-type human TTR and mutant P55 variant of human TTR, in the presence of Stimune adjuvant (Thermo Scientific, Waltham, MA, USA). After 46 and 50 days peripheral blood lymphocytes from individual llamas were isolated and total

RNA was extracted, converted into complementary DNA (cDNA), and cloned in a phagemid vector to generate two VHH phage display libraries as previously described (Harmsen *et al.* 2009). Bacteriophage displaying Nanobodies were selected after two consecutive rounds of panning selection on the immobilized antigen mutant P55 variant of human TTR at 5 µg/mL. After primary screening by binding ELISA (1 µg/mL of coating antigen) and sequencing analysis 10 different Nanobody families were identified. Periplasmic extracts of some clones were evaluated for their capacity to bind both human and mouse wild-type TTR in a similar ELISA set up (1 µg/mL of coating antigens). Nanobodies 169F7 and 165C6 (anti-TTR Nanobody characterization under submission) revealed to be cross-reactive to mouse TTR. For this reason these clones were chosen to be further characterized as purified material and clone 169F7 chosen to be tested in the *in vivo* settings.

Anti-TTR and irrelevant Nanobody (anti-G protein of Rabies virus) purification

169F7 anti-TTR and irrelevant Nanobody were produced and purified as previously described (Terryn *et al.* 2014). Detailed description is available in supplemental information.

Recombinant TTR production and purification

Recombinant mouse and human TTR were produced in a bacterial expression system using *Escherichia coli* BL21 and purified as previously described (Almeida *et al.* 1997; Gomes *et al.* 2016).

Endotoxin removal

To remove endotoxins from recombinant TTR and anti-TTR/irrelevant Nanobody, a polymixin B column (Thermo Scientific) was used, as previously described (Gomes *et al.* 2016). Protein concentration was determined using the Bradford method for TTR and Nanodrop 1000 (Thermo Scientific) for Nanobodies, using specific mass extinction coefficient.

Binding ELISA assay

Anti-TTR Nanobody 169F7 binding assay was performed by ELISA. Plates were coated overnight with either recombinant human or mouse wild-type TTR at 1 µg/mL (100 ng/well) and blocked with 4% bovine serum albumin in phosphate-buffered saline (PBS) for 2 h at 25°C. 169F7 anti-TTR and irrelevant Nanobodies were diluted in 2% blocking buffer and incubated for 1 h 25°C with the coated antigen. Nanobody detection was performed using an anti-His (1 : 1000; Abcam, Cambridge, UK, RRID AB_307016) in combination with an anti-rabbit-horseradish peroxidase (HRP) (1 : 2500; Binding Site, Birmingham, UK). 2% ABTS was used to detect HRP activity, and signal was detected and quantified at 450 nm.

Intranasal administration of 169F7/ irrelevant Nanobody

We applied a technique already established and optimized by (Furrer *et al.* 2009) that optimized the time that the antibody stays in the nasal cavity. We confirmed the success of this technique, with slight modifications, by intranasal dosing 0.3% Evans Blue in 0.9% NaCl. Briefly, adult (3–6 months old, weighting between 20 and 41 g) male/female wild-type mice and transgenic mice (TTR KO) were deeply anesthetized with a mixture of ketamine/medetomidine and maintained at 37°C during administration and 30 min after. Mice were

placed in a supine position and a total of 40 µL of Nanobody (400 µg) were administered, through a Gilson pipette, 2 µL in each nostril at a time with 2 min intervals between each nostril, at a total of 40 min. After the 2 µL supine administration, the mice were put on lateral position to avoid any liquid to go to the respiratory or gastro-intestinal track (remaining in nasal mucosa) and to facilitate breathing. Time points refer to the time after the first nasal instillation. The death rate was 0. Four animals were used in each time point (Nb 169F7: 1 h and 6 h; Nb Rab-E8/H7: 1, 2, 4, 6, 8, 10, 12, and 24 h). Physical randomization was performed by doing a lottery with the ear plug numbers. We wrote in small papers the ear plugs numbers, folded and place them in a box, mix and then the first four numbers took were assigned to the Nb 169F7 group for the timepoint 1h, the next four to the Nb 169F7 group for the timepoint 6h, and so on for the other nanobodies administered and the different timepoints, before going to the animal facilities. The pre-established exclusion criteria used were: when levels of nanobody were undetectable, mice were excluded from the study (less than 10%). This criteria explains some sample size differences. To minimize animal suffering after surgeries, cages were moderately heated under an heating pad for 2h after surgery. Moreover, animals were checked if they recovered well from the anesthesia with surgery score sheets.

Intra-cerebro ventricular administration of 169F7 Nanobody

Intracerebroventricular injection of the Nanobody was performed as described previously (Chauhan *et al.* 2001; Gomes *et al.* 2011), with minor modifications. Briefly, adult (3–6 months old, weighting between 22 and 36 g) male/female wild-type mice (sv129) and transgenic mice (TTR KO) were deeply anesthetized with a mixture of ketamine (Vetoquinol, Lure Cedex, France) and medetomidine (Prodivet ZN, Lisboa, Portugal), placed in a stereotaxic apparatus (Stoelting, Wood Lane, IL, USA), and given a unilateral injection of 20 µg of Nanobody (in 5 µL of artificial cerebrospinal fluid, (Tocris, Bristol, UK)) into the right lateral ventricle region, using a 10 µL motorized syringe (Hamilton, Sigma, St Louis, MO, USA) after drilling a small hole with a surgical drill. The coordinates of injection were anterior–posterior: –0.22 mm, medial–lateral: –1.0 mm, and dorsal–ventral: 1.8 mm from bregma. Two minutes after the needle insertion, Nanobody was injected at a constant flow rate of 0.5 µL/min. The needle remained in place for an additional 2 min to prevent reflux of fluid after delivery. The body temperature of mice was maintained at 37°C during surgery and 30 min after the injection. The death rate was close to 0. Four animals were used in each time point (Nb 169F7: 1, 6, 12, and 24 h). Randomization was performed as in intranasal administration. The exclusion criteria used was the same as in intranasal delivery to minimize animal suffering after surgeries, bupivacaine was injected before final skin closure, soft food was given and cages were moderately heated under an heating pad for 2h after surgery. Moreover, animals were checked with surgery score sheets to assure wellbeing.

Tissue processing

Detailed description is available in supplemental information.

Nanobody quantification in brain extracts

The quantification of functional anti-TTR Nanobody 169F7 and irrelevant anti-rabies Nanobody in brain homogenates was performed by binding ELISA. For the anti-TTR Nanobody, plates were

coated overnight with human wild-type TTR (1 µg/mL) and blocked with 4% skimmed milk in PBS for 2 h 25°C. Samples were diluted in 2% blocking buffer and incubated for 1 h 25°C with the coated antigen. Matrix interference was verified by testing spiked Nanobodies in different dilutions of brain homogenates (ranging from 1/2 to 1/100). Nanobody detection was performed using an anti-VHH (Ablynx house produced) in combination with an anti-rabbit-HRP (BETHYL, Montgomery, TX, USA, RRID: AB_67265). The total amount of Nanobody in the samples was determined by a standard curve attained from a 1.7 serial dilutions of the same Nanobody. The linear range of the standard curve was determined using 4PL analysis (GraphPad Software Inc., San Diego, CA, USA) as 0.3–20 ng/mL. Concentrations of unknown samples were determined by interpolation from the standard curve. For each brain extract sample, two to five different dilutions were tested. Quantification was accepted when two consecutive dilutions showed values within the same range of magnitude and the final Nanobody concentration was determined as the average of these values. It was excluded that the presence of native mouse TTR in brain tissue interferes with the quantification of the 169F7 Nanobody. To normalize the Nanobody quantification, the total protein content was determined for each brain extract sample using Bradford Ultra Reagent (Expediton, Swavesey, UK). The final data are shown in ng Nanobody per mg total protein. Similar procedures were used for quantification of the irrelevant Nanobody. To quantify the amount of anti-rabies Nanobody in the homogenized brain tissues and plasma the Platelia TM Rabies II Kit from Bio-Rad Laboratories, Hercules, CA, USA (Cat number: 3551180) was used with some minor adjustments; the detection of the Nanobody was performed using the anti-VHH antibody (Terry *et al.* 2014). Quantification was performed blinded to outcome assessment by different experimenters.

Immunohistochemistry/immunofluorescence of CNS Samples

Tissue samples for immunohistochemistry were collected after mice were perfused with PBS and 4% paraformaldehyde. 5-mm-thick tissue sections were deparaffinated in HistoClear and hydrated in a descending alcohol concentration series. For Immunohistochemistry: Endogenous peroxidase activity was inhibited with 3% hydrogen peroxide (methanol). Blocking was performed with 4% fetal bovine serum and 1% bovine serum albumin in PBS. Primary antibodies used were: rabbit polyclonal anti-His tag (Abcam, RRID: AB_307016, 1 : 1000). Antibodies were incubated overnight at 4°C with blocking solution. Antigen staining was performed with a biotin–extravidin enzyme complex (ABC Elite Vectastain kit; Vector Laboratories, Burlingame, CA, USA). Sections were examined and pictures were taken with an Olympus DP71 light microscope with a digital 195 camera. For Immunofluorescence: After deparaffination, slides were incubated with Tris-buffer saline (TBS), antigen retrieval was performed with citrate buffer (5 min microwave, 10 min 37°C) and then permeabilized with 0.25% Triton X-100 in TBS solution for 10 min and rinsed in TBS 0.025% Triton X-100. Blocking was performed with 10% fetal bovine serum, plus 1% bovine serum albumin and 0.3 M glycine, in TBS, for 2 h at 25°C. Primary antibodies were always incubated overnight at 4°C, in TBS 1% bovine serum albumin (BSA). Secondary antibodies were incubated 1 h at 25°C. The slides were mounted in a fluorescent mounting medium (DAKO, Glostrup, Denmark) and imaging was performed on a laser scanning Confocal Microscope Leica SP2/SP5 AOBSE (Leica, Wetzlar, Germany),

using the 40×/63× oil objective. In each set of experiments the same batch of antibodies (primary and secondary) was used, and images were taken using the same settings, such as camera exposure times. Primary antibodies used were anti-TTR Nanobodies 169F7 and 165C6 (in house production), anti-His (1 : 1000; Abcam, RRID:AB_307016), anti-Lamp1 (Abcam, 1 : 1000, RRID: AB_300425), anti-NeuN (Chemicon, Merck-Millipore, Burlington, MA, USA) 1 : 500, RRID:AB_2298772), anti-choline acetyltransferase (Chemicon, 1 : 100, RRID:AB_2079751); as secondary antibodies Alexa Fluor 488 and 568 (1 : 750; Gibco, Life Technologies, Carlsbad, CA, USA) were employed.

Primary motor neuron cultures

Primary cultures of mouse motor neurons were prepared from spinal cords E12–E13 of wild type (WT), TTR KO mice embryos (129/svJ background), as previously described (Gingras *et al.* 2007; Conrad *et al.* 2011; Graber and Harris 2013). Detailed description is available in supplemental information. These neuronal cultures were performed using a serum-free medium (B27; Gibco, Life Technologies), which does not contain T4 or retinol-binding protein, TTR ligands. The following pre-established exclusion criteria were used: cell cultures with high % of cell death (> 30%) and/or neurite network undeveloped or damaged.

Immunocytochemistry

Motor neuron cells were fixed in 4% sucrose/paraformaldehyde and immunocytochemistry was performed as previously described (Gomes *et al.* 2016). Primary antibodies used were anti-His (1 : 250; Abcam, RRID:AB_307016), anti-Islet1 (1 : 50; Abcam, RRID:AB_10866454), anti-ChAT (1 : 100; Merk-Milipore, RRID: AB_2079751), anti-MsTTR (1 : 100, Custom-made antibody against mouse recombinant TTR, produced by Quantum Appligene, Illkirch, France); as secondary antibodies Alexa Fluor 488 and 594 (1 : 750; Gibco, Life technologies) were employed. The fluorescent dye Hoechst 33342 (RRID: CHEBI:5742, 0.5 µg/mL, 10 min, 25°C) was used to stain nuclei.

mRNA semi-quantification through Real-time PCR

Total RNA was extracted from 7 DIV cultured motor neurons using TRIzol Reagent (Thermo Fisher Scientific, Waltham, MA, USA), as previously described (Gomes *et al.* 2011, 2016). Oligonucleotides used for mTTR were as follows: forward 5'-AGCCCTTTGCCTCTGGGAAGA-3' and reverse 5'-TGCGATGGTGTAGTGGCGATGG-3'. 18s RNA was used as reference gene with the following primers: forward, 5'-AAATCAGTTATGGTTCCTTTGGTC-3' and reverse 5'-GCTCTAGAATTACCACAGTTATCCAA-3'. The annealing temperature was 60°C. Data analysis was performed using the ΔCP method (between target gene and reference gene). The experimental unit in qPCR was each individual culture (different breeding females in independent neuronal cultures) or mice.

Western blot analysis

Cultured motor neurons were homogenized in lysis buffer as already described in (Gomes *et al.* 2016). Total protein concentration was determined using the Bradford method. Before homogenization, culture conditioned medium was collected and with Vivaspin 10 KDa columns (GE Healthcare, Little Chalfont, UK), the media were concentrated and exchanged for PBS, before denaturation and

western blot analysis. 120 µg of protein was applied and separated by 4%/15% Tris-Glycine sodium dodecyl sulfate–polyacrylamide (SDS-PAGE) gel electrophoresis and transferred to a polyvinylidene difluoride (PVDF) membrane (GE Healthcare), using a wet system, with Tris/Glycine buffer (Bio-Rad). Membranes were blocked at least 1 h at 25°C in blocking buffer, 5% bovine serum albumin in PBS Tween-20 (PBST), and then incubated overnight at 4°C with primary antibodies diluted in blocking buffer, namely anti-TTR (Dako RRID:AB_2335696), anti-mouse TTR and Nanobody 165C6 [in house production, together with anti-His (Abcam, ab9108)]. Membranes were then incubated with anti-rabbit IgG-HRP (1 : 10 000; Binding Site) or anti-mouse IgG-HRP (1 : 5000; Binding Site), for 1 h at 25°C. Blots were developed using Immuno-Star WesternC Chemiluminescent kit (Bio-Rad) and exposed to Bio-Rad ChemiDoc XRS system or ECL Hyperfilm (GE Healthcare), if signal was too low. Quantitative analyses were performed using the Quantity One software or ImageLab from Bio-Rad® Laboratories. The experimental unit in western blot assays was each individual culture (different breeding females in independent neuronal cultures).

Statistical analysis

Data presentation and 'n' description is described in figure legends. A previous power analysis was performed to obtain a 25% difference (10% SD) among two groups, with 90–95% power and we obtain sample sizes between three and six animals or individual cultures. Statistical analysis of the results was performed using one-way analysis of variance (ANOVA) followed by Bonferroni multiple comparison test, when three groups were present. Unpaired Student's *t*-test was used when the comparisons were only between two groups. For both statistical analysis: ****p* < 0.001, ***p* < 0.01, **p* < 0.05, ns (not significant).

Results

Anti-TTR 169F7 Nanobody binds both human and mouse TTR

Anti-TTR Nanobodies were generated for use in CNS distribution studies in mice. Out of a panel of different anti-TTR Nanobodies, described in methods, Nanobody 169F7 was selected since it clearly bound the native conformation of both mouse and human TTR in ELISA, using an irrelevant Nanobody directed against Rabies G-protein (Rab-E8/H7) as negative control (Fig. 1a). Immunohistochemistry analysis confirmed that anti-TTR 169F7 Nanobody recognized mouse TTR in choroid plexus brain cells and Langerhans Islets in the pancreas where TTR is produced, without staining the same tissues derived from TTR KO mice (Fig. 1b).

Anti-TTR Nanobody distribution in TTR KO mice following intranasal delivery

First, we studied the brain delivery and CNS distribution of the Nanobody 169F7 in TTR KO mice via the intranasal route (Fig. 2a). In such animals, the distribution of the Nanobody is only influenced by the characteristics of the Nanobody and

non-specific interactions. A dose of 400 µg of the monovalent anti-TTR 169F7 Nanobody (15 kDa) was intranasally delivered using four mice for each time point. The quantification of TTR nanobodies in the different brain part tissue homogenates was done in an ELISA, detecting functional binding to TTR. We found that after intranasal delivery of 400 µg of 169F7, this Nanobody reached all brain areas in significant concentrations (Fig. 3 and Table S1), with the highest levels observed in olfactory bulb, the entry gate to the brain, and also in the ventral parts of the brain (brainstem, cerebellum). Moreover, we saw that 1 h after the intranasal delivery, the Nanobody was also present in the spinal cord (Fig. 3f). Taking into account that the time points were registered after the first instillation, and that the total time of intranasal delivery was 40 min, this experiment, together with an extended intranasal delivery study with anti-Rab-E8/H7 Nanobody (Figure S1) we can conclude that Nanobodies reach the brain and CSF very quickly, with a maximum concentration reached after 1–2 h (Fig. 3 and Figure S1).

Anti-TTR Nanobody distribution in TTR WT mice following intranasal delivery

When studying the brain uptake of anti-TTR Nanobody 169F7 in WT mice, we observed a similar overall pattern of CNS distribution in all brain areas (Fig. 3). Surprisingly, WT mice showed consistently lower amounts of free anti-TTR Nanobody in all brain areas when compared with TTR KO mice. This difference was more evident in the spinal cord (Fig. 3f), dorsal root ganglia (DRG) (Fig. 3g) and serum (Fig. 3h), where very little Nanobody at both 1 h and 6 h was detected, compared to KO TTR mice (AUC Fold difference – Table S1). Also in serum (Fig. 3h), lower concentration were measured at the investigated time points (1 and 6 h) after start of administration.

Since both serum and DRG contain high amounts of TTR protein we hypothesize here that in the presence of soluble TTR, anti-TTR Nanobodies are cleared more rapidly than when the target is not present. DRGs have been shown to be rich in TTR because of the uptake of protein in a megalin-mediated mechanism (Fleming *et al.* 2009) either from blood or CSF. As opposed to the blood–brain barrier in the CNS, the DRG and peripheral axons lack an efficient neurovascular barrier, which allows the easy diffusion of large molecular weight compounds in the interstitium surrounding the DRG neurons (Abram *et al.* 2006; Sapunar *et al.* 2012). Moreover it was recently shown that glial cells surrounding DRG's, also present in the ganglia, internalize and degrade TTR, without synthesizing it (Gonçalves *et al.* 2014). Regarding cerebellum neurons, they have been also described to have TTR either because of local synthesis (Stein and Johnson 2002), or possibly also because of contamination from adjacent choroid plexus cells or protein uptake from CSF.

In addition, our data suggested the presence of soluble TTR also in the spinal cord. Two observations support our

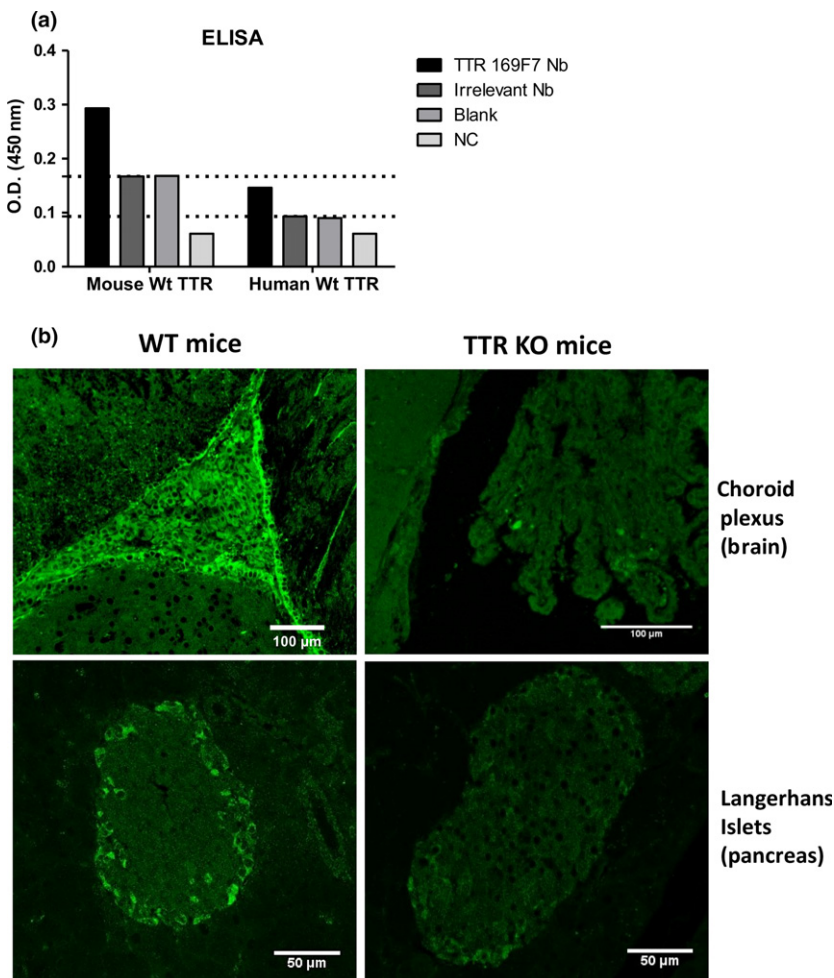


Fig. 1 Binding properties of anti-transthyretin (TTR) Nanobody 169F7. **(a)** Binding ELISA assay: 169F7 Nanobody binding to Mouse and Human TTR, and negative controls (irrelevant Nanobody, blank, no coating (NC); $n = 1$, $n =$ Nanobody binding to each TTR); **(b)** Representative immunofluorescence ($n = 3$, $n =$ IFs/animals, for each phenotype) of brain choroid plexus (CP) and pancreas Langerhans Islets, from wild type (WT) and TTR KO mice, stained against 169F7 Nanobody, using an anti-His tag antibody. Scale bar correspond to 100 μm in CP and to 50 μm in Pancreas.

hypothesis that soluble TTR in the brain and spinal cord explains the differences observed between TTR KO and WT mice. First, the presence of mouse TTR in brain tissue from WT mice did not interfere in the detection and quantification of the 169F7 Nanobody in the ELISA, which used human TTR to capture the 169F7 Nanobody (data not shown), indicating that the observed lower concentrations are not because of an assay artifact. Second, intranasal administration of a Rabies virus specific Nanobody in TTR WT mice gave similar distribution pharmacokinetics when compared with 169F7 in TTR KO mice (Table S1 and Figure S1). The molecular weight/size difference between the Rabies Nanobody (30 kDa) and the 169F7 Nanobody (15 kDa) might slightly influence diffusion kinetics.

Anti-TTR Nanobody distribution in TTR KO and WT mice by ICV delivery

The TTR 169F7 Nanobody CNS distribution by ICV delivery was also assessed in both WT and TTR KO mice (Figs 2b and 4). To this end 20 μg of Nanobody in a volume of 5 μL was injected in the right lateral ventricle of the right hemisphere, and both brain halves were collected at different time points to

assess the diffusion of the Nanobodies once in the brain. We found that the Nanobody was distributed to olfactory bulb, cerebrum, brainstem, and hippocampus (Fig. 4a–c and e). In agreement with intranasal delivery studies, we found that TTR-rich areas such as cerebellum, DRG, CSF, and serum as well as spinal cord contained lower amounts of Nanobody when comparing WT with KO mice (Fig. 4d and f–i and Table S2, for AUC fold difference). Thus, different routes of delivery yielded very similar differences in Nanobodies found in the brain from TTR KO and WT mice.

Anti-TTR Nanobody is specifically internalized in WT neuronal-like cells from the spinal cord

Since spinal cord emerged as one area where a clear difference was seen in anti-TTR Nanobody levels between WT and TTR KO mice, we sought to identify the source of these differences. Immunohistochemistry was performed on spinal cord sections from both WT and TTR KO ICV injected mice (1 h after injection), and anti-TTR Nanobody was detected via the C-terminal His-tag (Fig. 5a and b). We found that anti-TTR Nanobody was binding specifically to large neuronal-like cells in WT mice spinal cord, whereas in

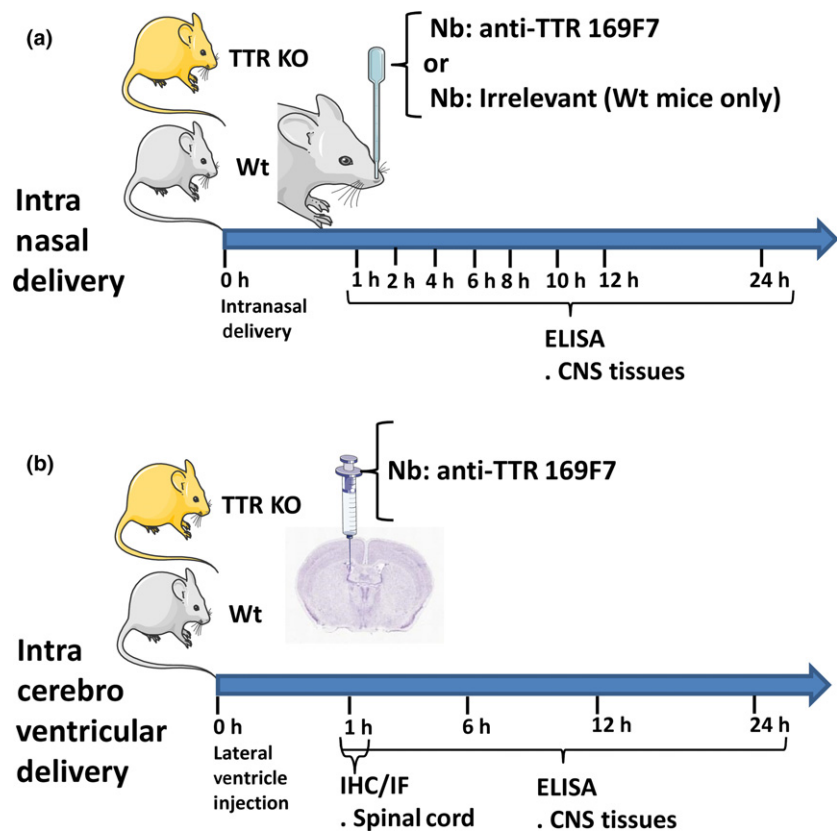


Fig. 2 Graphical time-line of experimental procedure for Nanobody delivery to CNS through Intra-nasal (IN) and Intra-cerebroventricular (ICV) delivery, in mice. (a) IN of 169F7 Nb and irrelevant Nanobody to Sv129 mice. 169F7 Nb was delivered to Wt and KO TTR mice, whereas Irrelevant Nb (Rab-E8/H7) to Wt mice only. Complete kinetics study with all time points was performed for irrelevant Nb, whereas for anti-TTR Nb to selected time points (1 and 6 h), (b) ICV of anti-TTR 169F7 Nanobody to Wt and TTR KO mice. Complete kinetics was performed with all time points indicated. Immunohistochemistry and immunofluorescence was performed in spinal cord of animals ICV injected 1 h post injection. For further details, see methods section (IN and ICV delivery).

the TTR KO mice the Nanobody seemed to be non-specifically internalized by all cells. Also, in TTR KO mice, the Nanobody was scattered in both white and gray matter, whereas in the WT mice the Nanobody was partially found in the white matter and in the large neuronal-like cells in the gray matter [Fig. 5a and b – IHC (immunohistochemistry) (same time of exposure)].

To understand if the Nanobody was specifically internalized by the neuronal-like cells (via receptor-mediated endocytosis) or was being internalized for degradation (pinocytosis), we co-localized the anti-TTR Nanobody (anti-his) with a lysosomal marker (anti-lamp1) using immunofluorescence microscopy. We found a clear difference in lysosomal uptake in most spinal cord cells of the TTR KO mice, and not on the WT mice, possibly indicating that the Nanobody is non-specifically degraded in TTR KO mice (Fig. 5a and b – IF). In WT mice, the anti-TTR Nanobody can bind to TTR for receptor-mediated internalization via pathways that do not lead to rapid degradation. Moreover, we observed that Nanobody was evenly distributed in the WT neuronal-like cells whereas, in TTR KO mice, the Nanobody was highly aggregated and clustered inside the cells, co-localizing with lamp1 (Fig. 5b).

In agreement with these results choroid plexus (extensively described as expressing and secreting TTR) of Wt and KO TTR Nb injected (ICV 1 h) animals, showed that anti-TTR

Nanobody is internalized by Wt Choroid cells, but not by KO TTR cells (Fig. 5c and d).

To understand if TTR was only being metabolized by these neuronal-like cells in the spinal cord and/or if these cells were also synthesizing TTR, we performed immunohistochemistry in WT non-injected mice, using a different anti-TTR Nanobody (165C6 – high affinity binder to mouse TTR, results under submission). We found that this anti-TTR Nanobody was able to recognize the same neuronal-like cells (Fig. 6a–c), suggesting that TTR is synthesized in these cells. In addition, TTR mRNA was detected in the spinal cord of Wt mice (Fig. 8b).

TTR-positive neuronal-like cells from the spinal cord are Motor neurons

Since TTR was shown to be synthesized in very small amounts in hippocampal/cortical neurons (Li *et al.* 2011) and also to be immunoreactive to a TTR antibody in human spinal cord motor neurons (Ranganathan *et al.* 2005), we investigated whether the neuronal-like cells that specifically bind and internalize anti-TTR Nanobodies were indeed motor neurons. For that, we performed co-localization studies using two motor neurons markers, anti-choline acetyltransferase (Fig. 7a) and anti-NeuN (Fig. 7b), and found that the neuronal-like cells co-localize with both motor neurons markers. To confirm that motor neurons could internalize the anti-TTR Nanobody and the complex anti-

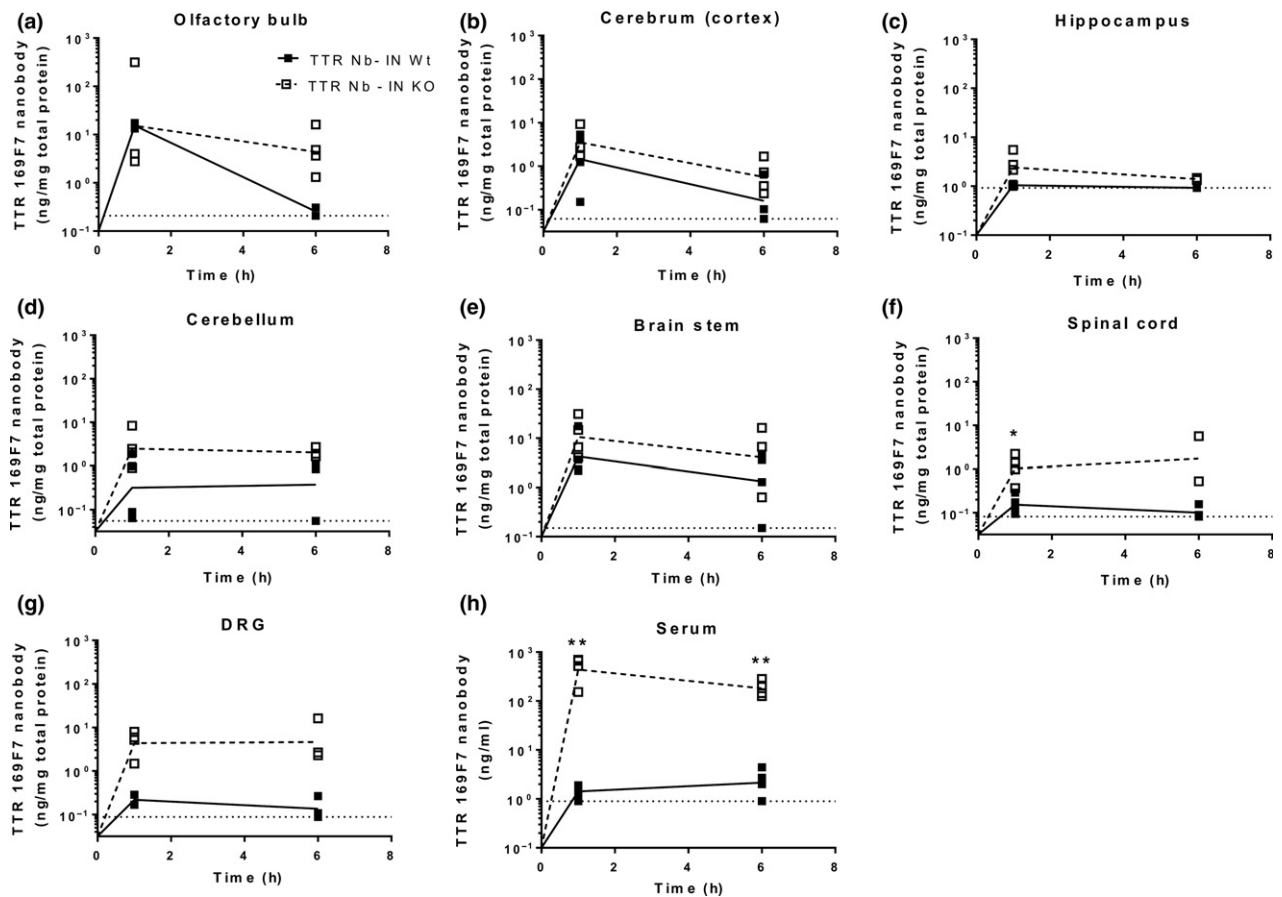


Fig. 3 Intranasal delivery of anti-transthyretin (TTR) Nanobody 169F7 to Wild Type and TTR KO mice. (a–h) Binding ELISA quantification of 169F7 anti-TTR Nanobody in different brain regions after intranasal delivery of 400 μ g in wild type (WT) and TTR KO mice at time points 1 and 6 h. The lower limit of quantification (LOQ) for TTR Nanobody was between 2–5 ng/mL. Nanobody concentrations were

normalized to total protein content. Data presented show all the replicates and a connecting line with the mean values, of $n = 2$ –4, for each time point ($n =$ mice/per time point). Statistical analysis was performed using Student's unpaired t-test for two groups only analysis. $**p < 0.01$, $*p < 0.05$, as compared the same time point between WT and TTR KO mice.

TTR Nanobody/TTR protein, *in vitro* cultures of motor neurons from WT mice were stimulated with recombinant mouse TTR (55 μ g/mL), which corresponds to TTR concentration in CSF, and/or anti-TTR 169F7 Nanobody (2 μ M) (Fig. 7c). We observed, through detection of the Histidine tag in the Nanobody by immunocytochemistry, that both Nanobody alone and Nanobody/TTR complex are specifically internalized by the motor neurons, indicating that TTR could also be in the culture media, as observed *in vivo*.

WT cultured Motor neurons synthesize and secrete TTR: mRNA and protein

To understand if motor neurons synthesize/secrete TTR or only internalize/metabolize TTR, we cultured motor neurons from both WT and TTR KO mice (7 DIV) (Gingras *et al.* 2007). These *in vitro* cultures are serum-free (supplemented with B27, Life technologies) and have minimal glial contamination, as the representative immunocytochemistry

in Fig. 8(a) shows. Almost all cells stain for motor neurons markers: choline acetyltransferase (ChAT) and Islet 1, with exception of some glial cells (indicated in the figure by an arrow) (Gingras *et al.* 2007; Conrad *et al.* 2011). Regarding TTR mRNA levels, we found, that TTR was expressed in both spinal cord tissue and motor neuron cultures. Moreover, a clear enrichment on TTR mRNA (30 fold) on motor neurons cultures was observed, compared to spinal cord levels (Fig. 8b). Regarding TTR protein levels, we used 2 antibodies and the 165C6 anti-TTR Nanobody. All indicated the presence of at least one band, if not two bands; with a similar size to mouse TTR protein present in WT serum and similar to recombinant mouse TTR (Fig. 8c). The difference in size, around 2 kDa might be because of the signal peptide of the intracellular mouse TTR produced in motor neurons or by different glycosylation profiles, as described for TTR (Teixeira and Saraiva 2013). The 165C6 anti-TTR Nanobody clearly identified the protein in WT cultured motor neurons,

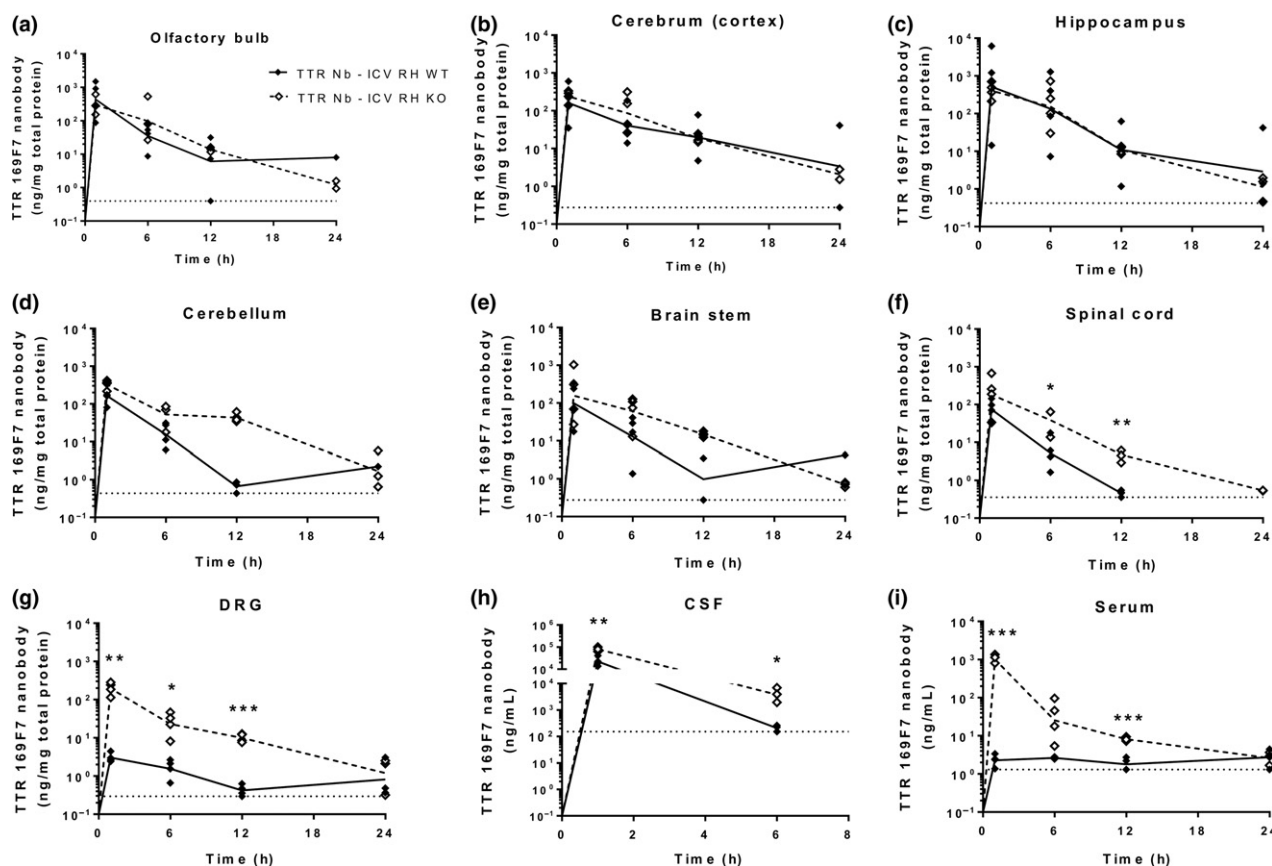


Fig. 4 Intra-cerebro ventricular (ICV) delivery of anti-transferrin receptor (TTR) Nanobody 169F7 to wild type (WT) and TTR KO mice. (a–i) Binding ELISA quantification of 169F7 anti-TTR Nanobody in different brain regions (right hemisphere a–e) after ICV delivery of 20 μ g in WT and TTR KO mice. The lower limit of quantification (LOQ) for TTR Nanobody was between 2 and 5 ng/mL. Nanobody concentrations

were normalized to total protein content. Data presented show all the replicates and a connecting line with the mean values, of $n = 2–4$, for each time point ($n =$ mice/per time point). Statistical analysis was performed using Student's unpaired *t*-test for two groups only analysis. *** $p < 0.001$, ** $p < 0.01$, * $p < 0.05$, as compared the same time point between WT and TTR KO mice.

but not in the KO TTR cultured motor neurons (Fig. 8c). Moreover, we found that TTR was being secreted by WT motor neurons in cultured conditioned media, and has a similar molecular weight, as compared to serum TTR (Fig. 8d). To understand where TTR protein was located in the highly polarized motor neurons, an immunocytochemistry was performed, using a rabbit anti-mouse TTR custom-made, which was the only antibody that specifically differentiated WT from TTR KO neuronal cultures. As the representative image shows, we observed that TTR protein is mainly in the neurites (Fig. 8e).

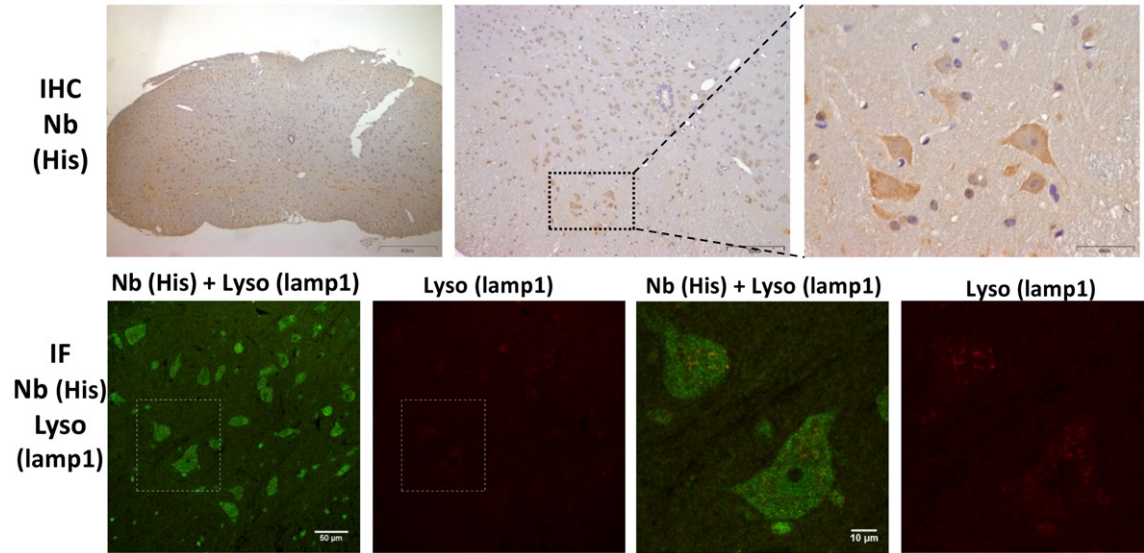
Discussion

In this work, we generated for the first time a Nanobody that recognized both human and mouse TTR. This Nanobody was efficiently delivered to the CNS, using a non-invasive route (intranasal delivery), describing its kinetics for the first time. Our data clearly show that Nanobodies can be efficiently

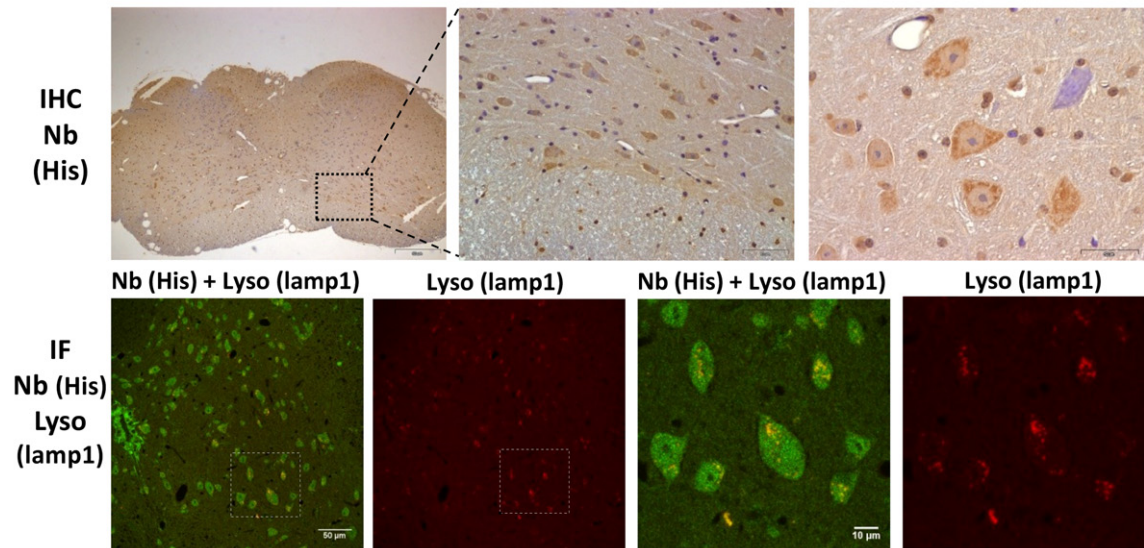
delivered to CNS, surpassing the BBB. In addition, using the anti-TTR nanobody as a specific functional tracer, we unraveled motor neurons in the spinal cord as a new cell type that synthesizes and secretes TTR, a novel finding that might be important in the understanding of the TTR biology with implications in the pathophysiology of some diseases such as amyotrophic lateral sclerosis since motor neurons are key elements of the disease and TTR was shown to be altered in the CSF of ALS patients.

Nanobodies are broadly applicable especially for the development of therapeutics and *in vivo* diagnostics, and their small size and favorable biophysical and biochemical properties allow them to penetrate and diffuse tissues very rapidly and efficiently (Hassanzadeh-Ghassabeh *et al.* 2013). Nevertheless, despite their small size, Nanobodies have low intrinsic capacity to cross the BBB when systemically administered (Terry *et al.* 2014) just like conventional antibodies. However, a few VHH have even been reported to cross the blood–brain barrier *in vivo* after peripheral

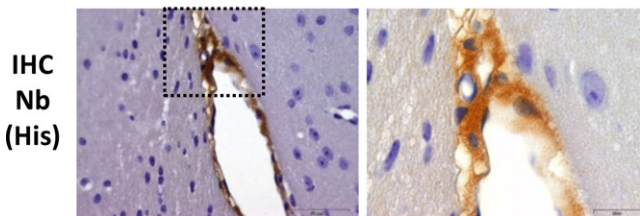
(a) ICV 1 h – Wt mice – Spinal cord



(b) ICV 1 h – TTR KO mice – Spinal cord



(c) ICV 1 h – Wt mice – Choroid Plexus



(d) ICV 1 h – KO TTR mice – Choroid Plexus

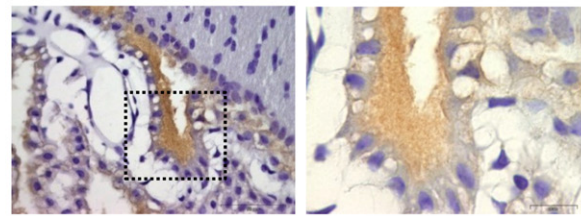


Fig. 5 Anti-transthyretin (TTR) Nanobody 169F7 is specifically internalized in spinal cord neuronal like cells. Representative immunohistochemistry (n = 3) and immunofluorescence (n = 3) (n = animal/for phenotype, in independent preparations) of the spinal cord of wild-type mice **(a)** and TTR KO mice **(b)** 1 h after intracerebroventricular (ICV) delivery of 20 μg of 169F7 Nanobody. Antibodies anti-His and anti-lamp1 were used to detect the Nanobody and

lysosomes, respectively. Representative immunohistochemistry (n = 3) (n = animal/for phenotype, in independent preparations) of the brain choroid plexus of wild-type mice **(c)** and TTR KO mice **(d)** 1 h after ICV delivery of 20 μg of 169F7 Nanobody. Antibodies anti-His was used to detect the Nanobody. Scale bar in IF correspond to 50 μm and 10 μm whereas in IHC to: (a) 1000 μm, 100 μm, and 50 μm; (b) 1000 μm, 50 μm, and 50 μm; (c) and (d) 50 μm.

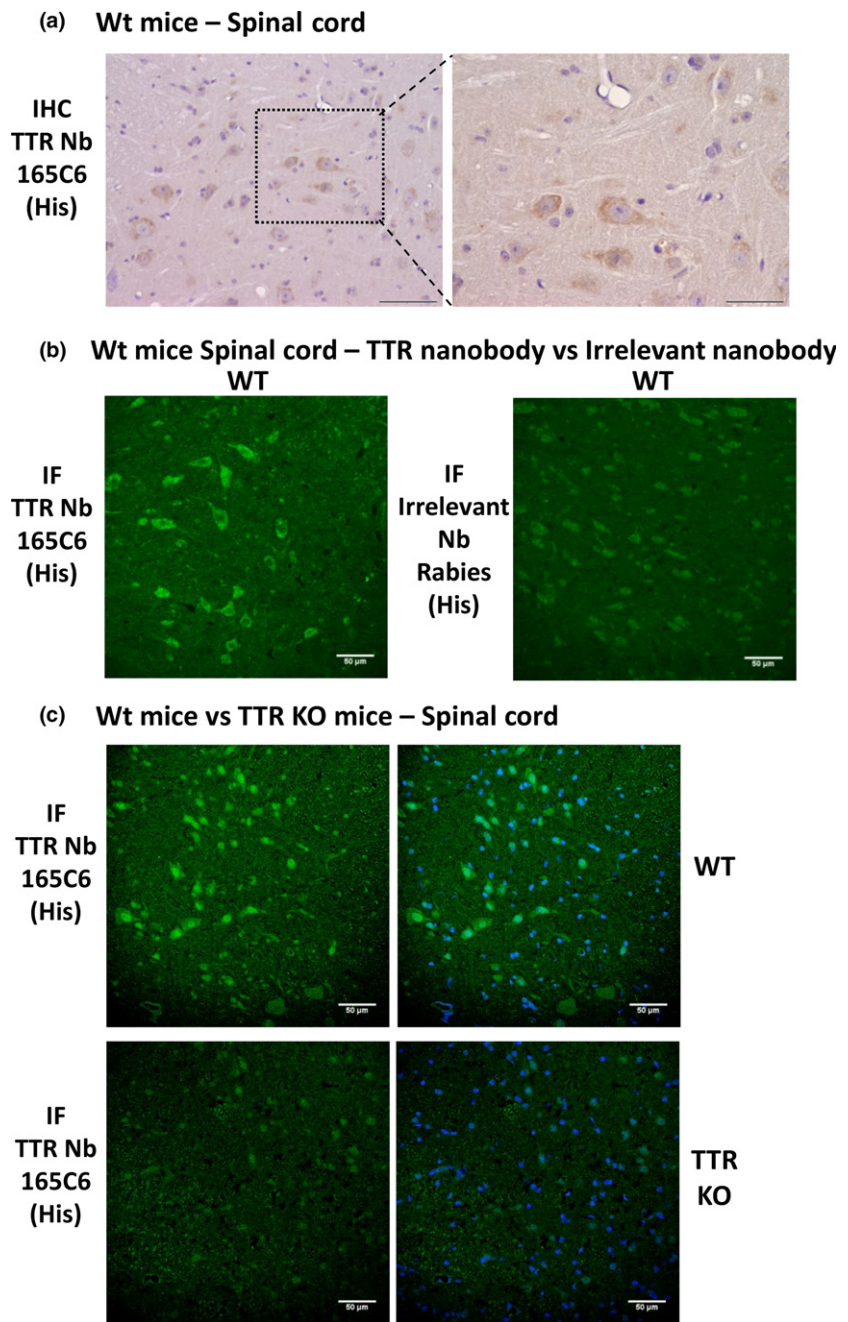


Fig. 6 Anti-transthyretin (TTR) Nanobody 165C6 specifically identifies neuronal like cells in non-injected wild type (WT) spinal cord mice. Representative immunohistochemistry ($n = 3$) and immunofluorescence ($n = 3$) ($n =$ animal/for phenotype, in independent preparations) of spinal cord of wild-type mice, non-injected with Nanobodies, stained against TTR with Nanobody 165C6 in optical IHC (a) and immunofluorescence, using an irrelevant Nanobody (b) and TTR KO mice (c) as negative controls. Scale bar in IHC corresponds to 100 μm and 50 μm and in IF corresponds to 50 μm .

injection, without the need of any invasive or hazardous procedures. It is hypothesized that this BBB crossing capacity depends on a basic isoelectric point and/or on the exposed charge on the surface of the nanobody. Such brain crossing Nanobodies have been identified and developed mainly for imaging purposes or therapeutic applications. The Nanobodies used in this study, however, have a pI of 6.18 (TTR Nanobody) and 5.97 (rabies Nanobody).

Here we demonstrate that Nanobodies can be efficiently used to target CNS using a non-invasive intranasal delivery method. Nanobodies quickly reached all areas of the brain

with the highest levels observed in the olfactory bulb, the entry gate to the brain, and the ventral parts of the brain (brainstem, cerebellum). Moreover, the Nanobody was also detected in the spinal cord. Even though we have not assessed it directly for TTR Nanobody, the distribution studies with the control rabies Nanobodies (Figure S1) indicate that two nasal passages were used by the Nanobody to reach the brain, the olfactory and peripheral trigeminal system, including the rapid extracellular route and the slower perineural route as reported before in other intranasal studies (Thorne *et al.* 2004; Furrer *et al.* 2009; Lochhead and

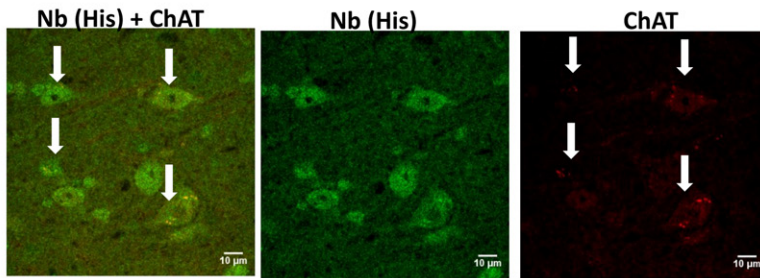
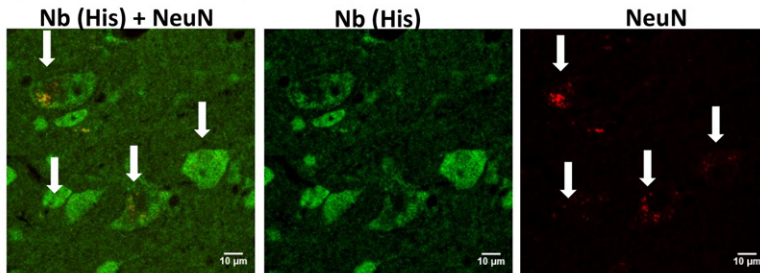
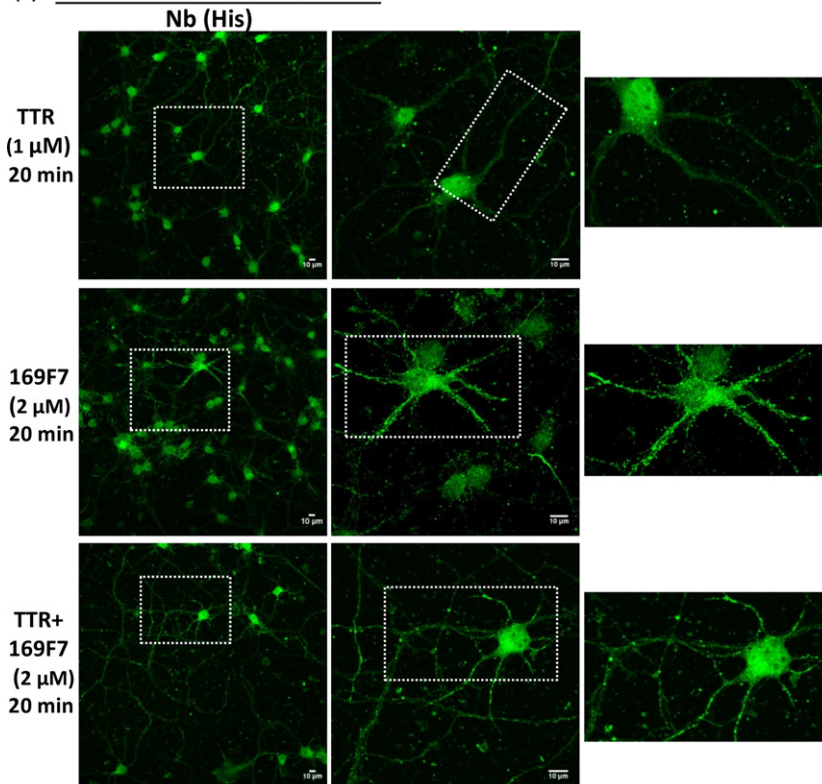
(a) ICV 1 h – Wt mice– Spinal cord**(b) ICV 1 h – Wt mice– Spinal cord****(c) Ex-vivo Motor Neuron culture**

Fig. 7 Wild-type (WT) neuronal like cells that are transthyretin (TTR) positive are motor neurons. Representative immunofluorescence ($n = 3$, $n =$ animals, in independent preparations) of the spinal cord of wild-type mice, 1 h after intracerebroventricular (ICV) delivery of 20 μg of 169F7 Nanobody. Antibodies anti-His (green) and anti-choline acetyltransferase (Chat) (a) or NeuN (red) (b), were used to detect the Nanobody and motor neurons (Chat, NeuN), respectively. (c) Primary motor neuron culture (7 DIV) of wild-type mice were stimulated with either MsTTR (55 $\mu\text{g}/\text{mL}$), 169F7 (2 μM) or both (previously pre-incubated) for 20 min. Representative immunofluorescence ($n = 3$, $n =$ independent cultures, in independent preparations) using an antibody anti-His was used to detect the Nanobody in the motor neurons.

Thorne 2012). ICV Nanobody delivery despite being an invasive strategy is a more efficient manner to deliver a compound to all the brain areas, being the difference more extensive in the dorsal areas of the brain (Fig. 4).

Regarding the kinetics of anti-TTR Nanobody delivery to the CNS in WT and TTR KO mice, we observed similar results between intranasal and ICV delivery, the results in the

TTR KO animals were in line with the CNS distribution of the rabies Nanobody used as irrelevant control. However, a strong difference between both animals strains was evident in TTR-rich areas such as the cerebellum and DRG, with WT mice showing less free TTR Nanobody, indicating that the complex TTR/Nanobody was being internalized through target binding. Surprisingly, the spinal cord also showed

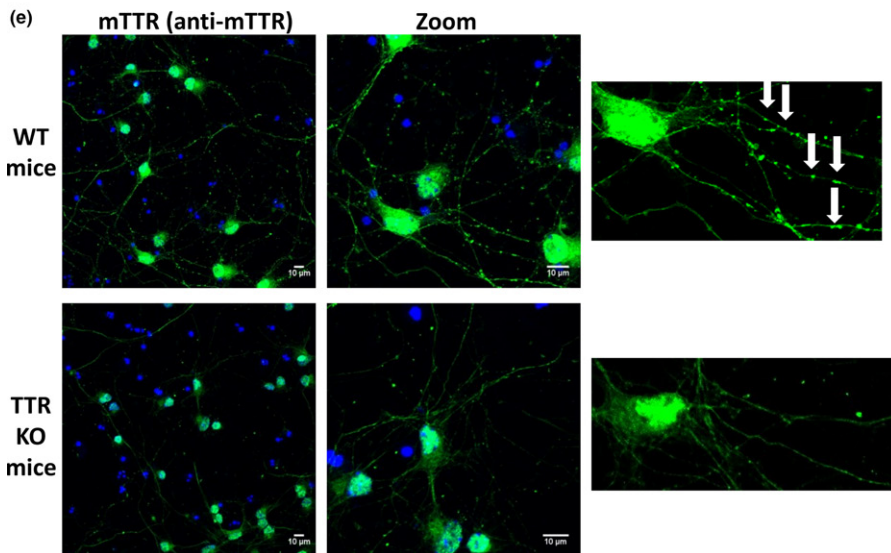
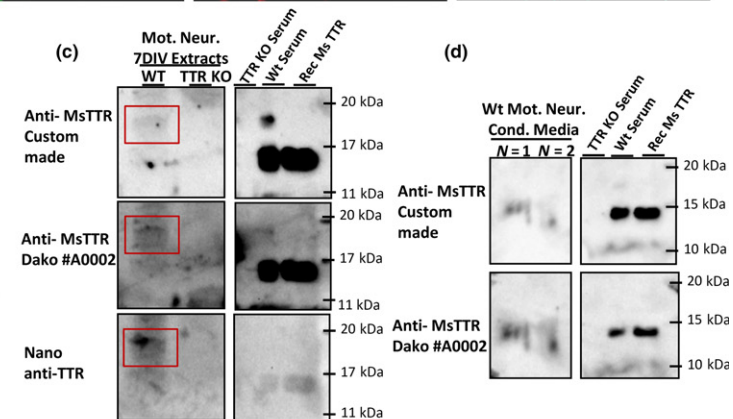
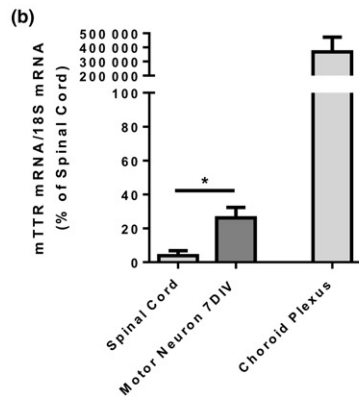
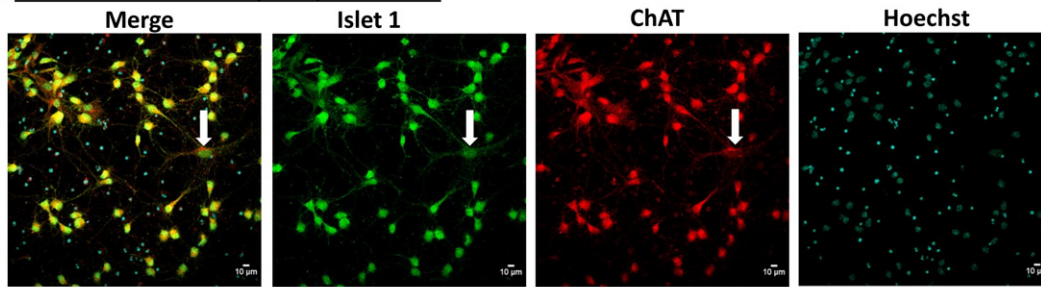
(a) Motor neuron culture (7DIV) – WT mice

Fig. 8 Wild-type (WT) Motor neurons synthesize and secrete transthyretin (TTR). (a) Representative immunofluorescence ($n = 3$, $n =$ independent cultures, in independent preparations) of primary motor neuron cultures (7 DIV) of wild-type mice. Antibodies anti-Islet-1 (green) and anti-choline acetyltransferase (Chat - red) were used to confirm the motor neuron phenotype (arrow points to the exception: one glial cell not staining any of the motor neurons markers); (b) Total RNA was extracted from spinal cord, choroid plexus, and primary motor neuron culture (7 DIV) of wild-type mice. TTR and 18S mRNA were semi-quantified through real-time PCR. Data represent the means \pm SEM of $n = 3$ –4 independent animals, or independent cultures; (c) Representative images of western blot analysis of $n = 2$ ($n =$ independent cultures and western blots), using two antibodies

against mouse TTR and anti-TTR Nanobody 165C6, in 7 DIV primary motor neuron extracts of wild-type mice, using recombinant mouse TTR protein and serum from WT mice as positive controls and TTR KO primary motor neuron cultures and serum from TTR KO mice as negative controls; (d) Representative images of western blot analysis of $n = 2$ ($n =$ independent cultures and western blots) from 7 DIV primary motor neuron conditioned medium of wild-type mice, using anti-TTR Nanobody 165C6; (e) Representative immunofluorescence ($n = 3$, $n =$ independent cultures and immunocytochemistry's) of primary motor neuron culture (7 DIV) of wild-type and TTR KO mice, stained against anti-mouse TTR, indicating positive staining for TTR in the neurites. Scale bars in motor neuron cultures correspond to 10 μ m.

statistically different lower amounts in WT versus TTR KO mice, suggesting spinal cord as a TTR-rich tissue, either through uptake or through direct synthesis of TTR (Figs 3 and 4; Tables S1 and S2).

Zooming into the spinal cord, we demonstrated that neuronal-like cells specifically internalized the anti-TTR 169F7 Nanobody *in vivo*. The Nanobody was distributed uniformly in these cells, internalized in a receptor-mediated process, most probably through megalin, a TTR receptor (Fleming *et al.* 2009; Gomes *et al.* 2016). Using neuronal markers we demonstrated that these cells are motor neurons (Kato *et al.* 1985; Gingras *et al.* 2007) (Fig. 7). In contrast, in TTR KO mice the 169F7 Nanobody was found in other cell types, where it accumulated in Lamp-1 positive lysosomes.

Immunohistochemistry demonstrated that in spinal cord, from non-injected mice, neuronal-like WT cells were recognized by another TTR-specific Nanobody, 165C6 (Fig. 6). Moreover TTR mRNA was detected in the spinal cord of the same non-injected Wt mice (Fig. 8b), summing one more evidence to the *in vivo* TTR synthesis by motor neurons. *In vitro* motor neuron cultures derived from WT mice engulf the anti-TTR Nanobody; when added, surprisingly this occurred even if no TTR protein was added to the cultures, and raising the question, that endogenous TTR could already be present in the culture condition media. This was in fact demonstrated through western blot; motor neurons express and secrete TTR protein into culture media. We could also show *in vitro*, that motor neurons synthesize TTR mRNA and that TTR is localized in the neurites, which is in agreement with its role in neuroprotection in CNS (Blay *et al.* 1993; Gomes *et al.* 2016) and in peripheral nervous system (Fleming *et al.* 2009). On the basis of the *in vitro* and *in vivo* observations we conclude that motor neurons in the spinal cord are a novel source of TTR production. Furthermore, it seems that these cells are not only secreting TTR, but are also engulfing TTR when complexed with the 169F7 Nanobody.

The absence of TTR, in KO TTR mice, has been shown to induce sensorimotor deficits, from locomotor activity to limb clasping phenotype (Fleming *et al.* 2007), but this phenotype has been only attributed to the sensory neurons (Fleming *et al.* 2009). Here we hypothesize that this phenotype could be related with TTR secretion from motor neurons since motor activity not only relies on the sensory system but also in the motor neurons. Unraveling that motor neurons synthesize/secrete TTR protein opens news questions in ALS pathology, as this is a motor neuron degeneration disease. TTR KO mice axons from sensory neurons show lower levels of retrograde transport described *in vitro* and *in vivo* (Fleming *et al.* 2009), which might also be happening in the axons of the motor neurons, affecting its retrograde transport and neurite outgrowth, therefore affecting the trophic support (Gomes *et al.* 2016). Moreover, TTR was shown to be altered in the CSF of ALS patients

(Ranganathan *et al.* 2005; Brettschneider *et al.* 2010; Ryberg *et al.* 2010), either being down-regulated with slow progression of the disease or up-regulated with a fast progression of the disease. Ranganathan *et al.* (2005) observed through immunohistochemistry that human motor neurons are targeted by an anti-TTR antibody, indicating that they possibly express TTR. In addition, they found that those same motor neurons, possibly expressing TTR in healthy donors, lose TTR stain in ALS patients, indicating a reduction in TTR synthesis or accelerated clearance. Another crosstalk between TTR and one of the mechanisms behind ALS pathology is glutamate excitotoxicity, since TTR has shown to be neuroprotective in neuronal excitotoxic models (Gomes *et al.* 2016). These findings might also shed some light to some rare familial amyloid polyneuropathy patient cases described to present atypical lower motor neuron diseases, similar to ALS. These patients present early features of lower motor neuron involvement with no tactile and thermo-dolorific sensory loss (Ando *et al.* 1993; Yoshioka *et al.* 2001; Salvi *et al.* 2003, 2014).

All combined, these discoveries recommend a closer insight of how TTR can regulate motor neuronal survival and/or neurite outgrowth/survival, taking into consideration not only regular physiological conditions but also ALS affected motor neurons.

Acknowledgments and conflict of interest disclosure

This work was supported by FEDER funds through the Operational Competitiveness Programme – COMPETE, by national funding from the Portuguese Foundation for Science and Technology (FCT) under the project PEst-C/SAU/LA0001/2011, QREN Brainiac 13141 and a post-doctoral fellowship (SFRH/BPD/84178/2012) to João Gomes. The authors acknowledge Paul Moreira for support in recombinant protein production and Paula Gonçalves, for tissue processing. The authors of the manuscript have the following potential competing interest: IC, HS, PV and, AW (left in 04/2012) were employees of ABLYNX at the time of work development. The other authors have no conflict of interests. The anti-TTR Nanobody discovery and characterization, as well as the quantification of Nanobodies in brain samples was performed by ABLYNX, whereas Nanobody delivery, tissue imaging, biochemistry processing as well as cellular cultures and data processing was performed by IBMC.

All experiments were conducted in compliance with the ARRIVE guidelines.

Supporting information

Additional Supporting Information may be found online in the supporting information tab for this article:

Figure S1. Intranasal delivery of irrelevant Nanobody (anti-Rabies G protein Nanobody).

Table S1. Nanobody concentrations parameters after intranasal delivery of anti-TTR Nanobody 169F7 and irrelevant Nanobody to WT and TTR KO mice (0-6h).

Table S2. Pharmacokinetics parameters after ICV delivery of anti-TTR 169F7 Nanobody to WT and TTR KO mice.

References

- Abram S. E., Yi J., Fuchs A. and Hogan Q. H. (2006) Permeability of injured and intact peripheral nerves and dorsal root ganglia. *Anesthesiology* **105**, 146–153.
- Almeida M. R., Damas A. M., Lans M. C., Brouwer A. and Saraiva M. J. (1997) Thyroxine binding to transthyretin Met 119. Comparative studies of different heterozygotic carriers and structural analysis. *Endocrine* **6**, 309–315.
- Alshehri B., D'Souza D. G., Lee J. Y., Petratos S. and Richardson S. J. (2015) The diversity of mechanisms influenced by transthyretin in neurobiology: development, disease and endocrine disruption. *J. Neuroendocrinol.* **27**, 303–323.
- Ando Y., Ueyama H., Watanabe S., Miyaji M., Tanaka Y., Ando M. and Araki S. (1993) Early involvement of motor nerve dysfunction in atypical cases with familial amyloidotic polyneuropathy (FAP) type I. *Muscle Nerve* **16**, 978–979.
- Andrade C. (1952) A peculiar form of peripheral neuropathy; familial atypical generalized amyloidosis with special involvement of the peripheral nerves. *Brain* **75**, 408–427.
- Blay P., Nilsson C., Owman C., Aldred A. and Schreiber G. (1993) Transthyretin expression in the rat brain: effect of thyroid functional state and role in thyroxine transport. *Brain Res.* **632**, 114–120.
- Brettschneider J., Lehmensiek V., Mogel H., Pfeifle M., Dorst J., Hendrich C., Ludolph A. C. and Tumani H. (2010) Proteomic analysis reveals candidate markers of disease progression in amyotrophic lateral sclerosis (ALS). *Neurosci. Lett.* **468**, 23–27.
- Buxbaum J. N., Ye Z., Reixach N. *et al.* (2008) Transthyretin protects Alzheimer's mice from the behavioral and biochemical effects of Abeta toxicity. *Proc. Natl Acad. Sci. USA* **105**, 2681–2686.
- Carro E., Trejo J. L., Gomez-Isla T., LeRoith D. and Torres-Aleman I. (2002) Serum insulin-like growth factor I regulates brain amyloid-beta levels. *Nat. Med.* **8**, 1390–1397.
- Chauhan N. B., Siegel G. J. and Lichter T. (2001) Distribution of intraventricularly administered anti-amyloid-beta peptide (Abeta) antibody in the mouse brain. *J. Neurosci. Res.* **66**, 231–235.
- Choi S. H., Leight S. N., Lee V. M., Li T., Wong P. C., Johnson J. A., Saraiva M. J. and Sisodia S. S. (2007) Accelerated Abeta deposition in APP^{sw}/PS1^{deltaE9} mice with hemizygous deletions of TTR (transthyretin). *J. Neurosci.* **27**, 7006–7010.
- Conrad R., Jablonka S., Szczepan T., Sendtner M., Wiese S. and Klausmeyer A. (2011) Lectin-based isolation and culture of mouse embryonic motoneurons. *J. Vis. Exp.* **55**, e3200 (1–4).
- Dhuria S. V., Hanson L. R. and Frey W. H., 2nd (2010) Intranasal delivery to the central nervous system: mechanisms and experimental considerations. *J. Pharm. Sci.* **99**, 1654–1673.
- Episkopou V., Maeda S., Nishiguchi S., Shimada K., Gaitanaris G. A., Gottesman M. E. and Robertson E. J. (1993) Disruption of the transthyretin gene results in mice with depressed levels of plasma retinol and thyroid hormone. *Proc. Natl Acad. Sci. USA* **90**, 2375–2379.
- Fleming C. E., Saraiva M. J. and Sousa M. M. (2007) Transthyretin enhances nerve regeneration. *J. Neurochem.* **103**, 831–839.
- Fleming C. E., Mar F. M., Franquinho F., Saraiva M. J. and Sousa M. M. (2009) Transthyretin internalization by sensory neurons is megalin mediated and necessary for its neurotrophic activity. *J. Neurosci.* **29**, 3220–3232.
- Furrer E., Hulmann V. and Urech D. M. (2009) Intranasal delivery of ESBA105, a TNF-alpha-inhibitory scFv antibody fragment to the brain. *J. Neuroimmunol.* **215**, 65–72.
- Gingras M., Gagnon V., Minotti S., Durham H. D. and Berthod F. (2007) Optimized protocols for isolation of primary motor neurons, astrocytes and microglia from embryonic mouse spinal cord. *J. Neurosci. Methods* **163**, 111–118.
- Gomes J. R., Lobo A. C., Melo C. V. *et al.* (2011) Cleavage of the vesicular GABA transporter under excitotoxic conditions is followed by accumulation of the truncated transporter in nonsynaptic sites. *J. Neurosci.* **31**, 4622–4635.
- Gomes J. R., Nogueira R. S., Vieira M., Santos S. D., Ferraz-Nogueira J. P., Relvas J. B. and Saraiva M. J. (2016) Transthyretin provides trophic support via megalin by promoting neurite outgrowth and neuroprotection in cerebral ischemia. *Cell Death Differ.* **23**, 1749–1764.
- Goncalves N. P., Costelha S. and Saraiva M. J. (2014) Glial cells in familial amyloidotic polyneuropathy. *Acta Neuropathol. Commun.* **2**, 177.
- Graber D. J. and Harris B. T. (2013) Purification and culture of spinal motor neurons from rat embryos. *Cold Spring Harb. Protoc.* **2013**, 319–326.
- Harmsen M. M., Fijten H. P., Engel B., Dekker A. and Eble P. L. (2009) Passive immunization with llama single-domain antibody fragments reduces foot-and-mouth disease transmission between pigs. *Vaccine* **27**, 1904–1911.
- Hassanzadeh-Ghassabeh G., Devoogdt N., De Pauw P., Vincke C. and Muyldermans S. (2013) Nanobodies and their potential applications. *Nanomedicine (Lond)* **8**, 1013–1026.
- Herce H. D., Schumacher D., Schneider A. F. L. *et al.* (2017) Cell-permeable nanobodies for targeted immunolabelling and antigen manipulation in living cells. *Nat. Chem.* **9**, 762–771.
- Kato M., Kato K., Blaner W. S., Chertow B. S. and Goodman D. S. (1985) Plasma and cellular retinoid-binding proteins and transthyretin (prealbumin) are all localized in the islets of Langerhans in the rat. *Proc. Natl Acad. Sci. USA* **82**, 2488–2492.
- Kawaji T., Ando Y., Nakamura M., Yamamoto K., Ando E., Takano A., Inomata Y., Hirata A. and Tanihara H. (2005) Transthyretin synthesis in rabbit ciliary pigment epithelium. *Exp. Eye Res.* **81**, 306–312.
- Li X., Masliah E., Reixach N. and Buxbaum J. N. (2011) Neuronal production of transthyretin in human and murine Alzheimer's disease: is it protective? *J. Neurosci.* **31**, 12483–12490.
- Lochhead J. J. and Thorne R. G. (2012) Intranasal delivery of biologics to the central nervous system. *Adv. Drug Deliv. Rev.* **64**, 614–628.
- Murakami T., Yasuda Y., Mita S., Maeda S., Shimada K., Fujimoto T. and Araki S. (1987) Prealbumin gene expression during mouse development studied by in situ hybridization. *Cell Differ.* **22**, 1–9.
- Power D. M., Elias N. P., Richardson S. J., Mendes J., Soares C. M. and Santos C. R. (2000) Evolution of the thyroid hormone-binding protein, transthyretin. *Gen. Comp. Endocrinol.* **119**, 241–255.
- Ranganathan S., Williams E., Ganchev P. *et al.* (2005) Proteomic profiling of cerebrospinal fluid identifies biomarkers for amyotrophic lateral sclerosis. *J. Neurochem.* **95**, 1461–1471.
- Ryberg H., An J., Darko S., Lustgarten J. L., Jaffa M., Gopalakrishnan V., Lacomis D., Cudkowicz M. and Bowser R. (2010) Discovery and verification of amyotrophic lateral sclerosis biomarkers by proteomics. *Muscle Nerve* **42**, 104–111.
- Salvi F., Scaglione C., Michelucci R. *et al.* (2003) Atypical familial motor neuropathy in patients with mutant TTR Ile68Leu. *Amyloid* **10**, 185–189.

- Salvi F., Rosaria P., Pastorelli F. and Rapezzi C. (2014) Familial amyloid polyneuropathy presenting as atypical lower motor neuron disease: a case report (P4.091). *Neurology* **82**, P4-091.
- Santos S. D., Lambertsen K. L., Clausen B. H., Akinc A., Alvarez R., Finsen B. and Saraiva M. J. (2010) CSF transthyretin neuroprotection in a mouse model of brain ischemia. *J. Neurochem.* **115**, 1434–1444.
- Sapunar D., Kostic S., Banozic A. and Puljak L. (2012) Dorsal root ganglion – a potential new therapeutic target for neuropathic pain. *J. Pain Res.* **5**, 31–38.
- Soprano D. R., Herbert J., Soprano K. J., Schon E. A. and Goodman D. S. (1985) Demonstration of transthyretin mRNA in the brain and other extrahepatic tissues in the rat. *J. Biol. Chem.* **260**, 11793–11798.
- Sousa J. C., Cardoso I., Marques F., Saraiva M. J. and Palha J. A. (2007) Transthyretin and Alzheimer's disease: where in the brain? *Neurobiol. Aging* **28**, 713–718.
- Stein T. D. and Johnson J. A. (2002) Lack of neurodegeneration in transgenic mice overexpressing mutant amyloid precursor protein is associated with increased levels of transthyretin and the activation of cell survival pathways. *J. Neurosci.* **22**, 7380–7388.
- Teixeira A. C. and Saraiva M. J. (2013) Presence of N-glycosylated transthyretin in plasma of V30M carriers in familial amyloidotic polyneuropathy: an escape from ERAD. *J. Cell Mol. Med.* **17**, 429–435.
- Terryn S., Francart A., Lamoral S. *et al.* (2014) Protective effect of different anti-rabies virus VHH constructs against rabies disease in mice. *PLoS ONE* **9**, e109367.
- Thorne R. G., Pronk G. J., Padmanabhan V. and Frey W. H., 2nd (2004) Delivery of insulin-like growth factor-I to the rat brain and spinal cord along olfactory and trigeminal pathways following intranasal administration. *Neuroscience* **127**, 481–496.
- Tsuzuki T., Mita S., Maeda S., Araki S. and Shimada K. (1985) Structure of the human prealbumin gene. *J. Biol. Chem.* **260**, 12224–12227.
- Wolfson W. (2006) Ablynx makes nanobodies from llama bodies. *Chem. Biol.* **13**, 1243–1244.
- Yoshioka A., Yamaya Y., Saiki S., Hirose G., Shimazaki K., Nakamura M. and Ando Y. (2001) A case of familial amyloid polyneuropathy homozygous for the transthyretin Val30Met gene with motor-dominant sensorimotor polyneuropathy and unusual sural nerve pathological findings. *Arch. Neurol.* **58**, 1914–1918.